ChemistrySelect

Research Article
doi.org/10.1002/slct.202303972

Chemistry Europe
European Chemical Societies Publishing

www.chemistryselect.org

Dissociation Constant of Di- and Tri-Basic Solvents Based on Piperazine and Its Derivatives for Post-Combustion CO_2 Capture

Mehul Darji,[a] Anu Manhas,[a] Sukanta K. Dash,*[b] and Kalisadhan Mukherjee*[a]

Amine solvents remain popular in the industries for post combustion carbon dioxide (CO_2) capture. Dissociation constant of basic amine solvents plays significant role to influence the CO_2 absorption. It is thus important to study the dissociation of new amine solvents for assessing their viability for CO_2 capture. In the present work, potentiometric titration method is employed to determine the dissociation constants of dibasic (e.g., Piperazine (PZ), 1-methyl piperazine (1-MPZ) and tribasic amines (1-(2-aminoethyl-piperazine) (AEPZ) which could be promising for formulating blended solvent system towards enhancing the rate of CO_2 absorption. The estimated dissociation constants for the PZ and 1-MPZ while match well with reported results, the dissociation constants for AEPZ has been determined newly here within the temperature range 298—318 K. In addition, the structural geometric parameters and Natural Bond Order (NBO) calculations of the amine solvents are performed based on Density Functional Theory (DFT). The NBO calculations predict charge distribution on the nitrogen and other elements, and envisage its effect on the pK_a values of the amines. Further, potential energy surface (PES) scanning calculations are performed for AEPZ to explain it's ring inversion which is responsible for obtaining a single pK_a value in experimental studies.

Introduction

The increase in atmospheric CO_2 and the associated global warming have evoked researchers to develop techniques for capturing CO_2.[1] Various techniques including but not limited to membrane separation, liquid absorbents/ solid adsorbents, cryogenic sorption, microbial algae system are already been exercised for CO_2 absorption purpose.[2] Many solid adsorbents including metal oxides, polymers, and bio-materials are used for the CO_2 capture process.[3] However, liquid amine solvents remain mostly popular for the absorption of industrial flue gas.[2b,4] The ability of basic amine solvents to bind acidic CO_2 chemically at low partial pressure has made them attractive for industrial use.[5] Liquid amines (RNH_2) under the exposure of CO_2 form carbamate ($RNHCOO^-$) and amine becomes protonated (RNH_3^+). Higher protonation of amine eventually leads to the larger CO_2 absorption. Alternatively, more the dissociation of protonated amine, lower will be the CO_2 absorption. The dissociation of protonated amines is temperature dependent and significantly influences the absorption of acidic gases.[6] It is thus important to assess the protonation behavior of amine solvents prior to carry out the CO_2 capture experiments. In our earlier publication, we have reviewed the literatures which report the estimation of dissociation constants for various solvents.[7] It seems that the estimation of dissociation constant for the new amine solvents is fundamental and technologically significant.

Recently Piperazine (PZ), 1-Methy Piperazine (1-MPZ), and 1-(2-aminoethyl-piperazine) (AEPZ) are used either a solvent mix or a reaction rate activator in blended solvents for CO_2 capture.[8] Dash et al.[9] have studied the VLE of CO_2 in various concentrations (3.2 M to 4.5 M) of PZ and reported it's promising CO_2 capture performances. Cullinane and Rochelle[10] have studied the kinetics of CO_2 absorption in PZ and found that 1 M PZ reacts with CO_2 faster than conventional solvent MEA. Li et al.[11] have studied CO_2 solubility in an aqueous 1-MPZ solution within the concentration range of 10–40 wt%, and reported that 30 wt% 1-MPZ has higher cyclic CO_2 absorption capacity than 10 wt% 1-MPZ. The kinetic study on the absorption of CO_2 in 1-MPZ is reported by Rayer et al.[12] They have shown that 1-MPZ blends with primary or secondary amine exhibit a higher rate of reaction with CO_2. Dey et al.[8a] have reported the CO_2 absorption in AEPZ and it's blend with 2-amino-2-methyl-1-propanol (AMP) by vapor liquid equilibrium (VLE) studies. Their study shows that the AEPZ and AEPZ-activated blend solvents have higher CO_2 absorption capacity than monoethanol amine (MEA) and it's blend with AMP. Dash and Sharma[8b] have studied the reaction kinetics of CO_2 with AEPZ and found a faster rate as compared to MEA. For the design of CO_2 capture process by chemical absorption, knowledge of physiochemical properties is essential. Although properties such as density, viscosity, solubility etc. are some-

[a] M. Darji, A. Manhas, K. Mukherjee
Department of Chemistry, Pandit Deendayal Energy University, Gandhinagar 382426, India
E-mail: kalisadhan.mukherjee@sot.pdpu.ac.in
kalisadhanm@yahoo.com

[b] S. K. Dash
Department of Chemical Engineering, Pandit Deendayal Energy University, Gandhinagar 382426, India
E-mail: sk.dash@sot.pdpu.ac.in
sukantakdash@gmail.com

Supporting information for this article is available on the WWW under https://doi.org/10.1002/slct.202303972

what available in the literature, data on dissociation constants are hardly reported. The dissociation constant of PZ and hydroxyethyl piperazine is investigated by Hemborg et al.[13] using the electromotive force technique at the temperature range between 293 to 353 K. The pK_a value of amine based absorbents (ethylenediamine, PZ, 1-(2-hydroxyethyl) piperazine, 1–4-bis (2-hydroxyethyl)piperazine, and 1-(2-hydroxyethyl)-4-(2-hydroxypropyl) piperazine) for SO_2 capture process have recently been measured by Wang et al.[14] using a mathematical model. Henni et al. and their group[15] have measured the $-\ln K_a$ value of various amine solvents (e.g.; DIPA, N,N,N′,N′-tetrakis (2-hydroxypropyl) ethylenedimine, 2-[[2-(dimethylamino) ethyl]methyl amino] ethanol, tris[2-(2-methoxyethoxy)ethyl] amine, N-(2-hydroxy)aniline, 1-(2-hydroxyethyl)piperazine, 1-MPZ, PZ, monoethanolamine (MEA), 1,4-bis(3-aminopropyl) piperazine, 1,3-bis(aminomethyl)-cyclohexane, tris(2-aminoethyl) amine, and 1-amino-4-methyl piperazine, etc.) with the help of potentiometric titration method. It is reported that 1-(2-aminoethyl) piperazine and its blend can be a potential candidate for CO_2 absorption process.[8] Although many properties of AEPZ and their blends are available in the literature, the dissociation constant which is an essential property is not reported so far. Hence, in this work the dissociation constant of AEPZ along with PZ and 1-MPZ have been determined using titrimetric method which is considered as simple and cost-effective technique for the estimation of the dissociation constant for amine solvents. The titration of amine with HCl produces protonated amine which again equilibrates with the corresponding amine following the reaction shown in Equation (1).

$$RNH_2 + H_3O^+ \leftrightarrow RNH_3^+ + H_2O \quad (1)$$

The procedures and protocols for estimating the dissociation constant (K_a) of protonated monobasic amine solvents using the potentiometric titration method are already reported by our research group elsewhere[7] and also discussed briefly in methodology section. Following similar protocols in the present work, we have reported dissociation constants of dibasic PZ, 1-MPZ and tribasic amines AEPZ. Usually, the number of nitrogen (N) atoms present in the amine predicts their basicity. Thus, mono, di and tri-basic amines are consisted of 1, 2 and 3 nitrogen (N) atoms respectively. For the titration of amines with HCl, the titration plot (pH vs volume of HCl added), should observe 1, 2 or 3 number steep pH changes corresponding to their single or multiple pK_a values. The estimated dissociation constants for the PZ and 1-MPZ while match well with reported results, herein, we are also reporting first time the values of the dissociation constant for AEPZ determined at five different temperatures (298–318 K). We also conducted electronic structure calculations to validate the experimental outcome. The selected amines are optimised at the ground state via Density Functional Theory (DFT) studies at B3LYP/6-311 + G(d, p) with IEFPCM solvent model. The lengths of various important bonds of the amines are calculated from the optimized geometry and the charge distribution among the nitrogen and other elements is estimated. Finally, DFT studies are used to validate the experimentally determined dissociation constant values of the investigated amines. Moreover, the reason of retrieving one experimental pK_a value instead of having three Nitrogen in the scaffold of AEPZ molecule has been explained via PES calculations of DFT studies. The justification of single pK_a of AEPZ was explained based on the ring inversion generated via PES calculations.

Reaction and Mechanism for CO_2 Absorption by Amine

The following reactions illustrate the general chemical processes involved in the adsorption of CO_2 in amine solvents.[16]

$$RNH_2 + CO_2 + H_2O \leftrightarrow RNHCOO^- + H_3O^+ \quad (2)$$

$$RNH_2 + H_3O^+ \leftrightarrow RNH_3^+ + H_2O \quad (3)$$

$$2RNH_2 + CO_2 \leftrightarrow RNHOO^- + RNH_3^+ \quad (4)$$

Equation (2) explains the formation of carbamate due to the interaction between CO_2 and amine (RNH_2). The subsequent formation of protonated amine due to the reaction between the amine and the acidic aqueous media is presented in Equation (3). The overall reaction for absorption of CO_2 in aqueous amine solvent is presented in Equation (4). Higher protonation of amine ultimately results larger CO_2 absorption. The CO_2 absorption within amine solvents (Equation (4)) proceeds even at low partial pressure and at low temperatures (~40 °C). At high temperatures the equilibrium of Equation (4) moves to the left, allowing for the recovery of the absorbed CO_2. Thus, in industrial processes, CO_2 is captured within an absorber column at low temperatures and released from desorber column at high temperature.[7]

Methodology

Theory for the Estimation of Dissociation Constant

To determine the dissociation constant's value, the PZ, 1-MPZ and AEPZ are titrated with HCl and the pK_a value is calculated using Equation (5) based on the acid-base reaction mentioned in Equation (1).[7,15b]

$$pKa = +log\frac{[RNH_3^+]}{[RNH_2]} \quad (5)$$

Typical dataset used for estimating the first and second pK_a value of PZ at 298 K are summarised in Tables 1 and 2 respectively.

The dissociation constant (K_a) follows the relationships with thermodynamic parameters △G (change in Gibbs free energy) and △H (change in enthalpy) as described in Equations (6) and (7).

Table 1. First pKa Values of PZ at 298 K.

HCl/ml	pH	$[PZH^+]/[PZ]$	$\log([PZH^+]/[PZ])$	pK_a ($-\log K_a$)
0	10.78			
0.42	10.5	0.11	−0.95	9.54
0.84	10.34	0.25	−0.60	9.73
1.26	10.09	0.42	−0.36	9.72
1.68	9.93	0.66	−0.17	9.75
2.1	9.73	1	0	9.73
2.52	9.45	1.50	0.17	9.62
2.94	9.08	2.33	0.36	9.44
3.36	8.19	4	0.60	8.79
3.78	6.73	9	0.95	7.68
4.2	6.29			
Avg. pK_a				9.33

Table 2. Second pKa values of PZ.

HCl/ml	pH	$[PZ2H^+]/[PZ]$	$\log([PZ2H^+]/[PZ])$	pK_a ($-\log K_a$)
4.2	6.29			
4.62	6.02	0.11	−0.95	5.06
5.04	5.86	0.25	−0.60	5.25
5.46	5.7	0.42	−0.36	5.33
5.88	5.5	0.66	−0.17	5.32
6.3	5.33	1	0	5.33
6.72	5.17	1.50	0.17	5.34
7.14	4.85	2.33	0.36	5.21
7.56	4.44	4	0.60	5.04
7.98	3.55	9	0.95	4.50
8.4	3.09			
Avg. pK_a				5.15

$$\Delta G = -RT\ln K_a \tag{6}$$

$$\Delta H = -R\frac{d\ln K_a}{d\left(\frac{1}{T}\right)} \tag{7}$$

where, R stands for gas constant, T is absolute temperature.

Experimental Methodology

Commercially available (Sigma-Aldrich/Finar) amines, e.g., PZ [CAS No.110-85-0], 1-MPZ [CAS No.109-01-3], and AEPZ [CAS No.140-31-8] are taken for the experiments. Aqueous solvents are prepared by weight. Table S1, Supporting Information provides an overview of the chemical composition, molecular weight, boiling point, and structures of these amines. The potentiometric titration to measure the dissociation constant is carried out using an auto titrator equipped with pH electrode (Orion Star 8172BNWP with accuracy up to 0.01). Prior to performing the titration, the molarity of titrant HCl (~0.1) is verified by standardizing with Na_2CO_3. The titration is carried out in the temperature range 298–318 K. Acid is added to amines till achieving the pH ~2.5 to ensure the completion of titration.[7] The pH electrode has been calibrated using a standard buffer solution (pH: 4.01, 7.00, 10.01) at each working temperature.

Computational Methodology

Density Functional Theory (DFT) studies are carried out on the cyclic amine solvents, i.e., PZ, 1-MPZ, and AEPZ and their protonated counterparts (PZH^+, $PZ2H^+$, $1\text{-}MPZH^+$, $1\text{-}MPZ2H^+$ and $AEPZH^+$) to validate the experimentally obtained $-\ln K_a$ values. Gausian 09 programme has been used to perform all the ground state (S_0) DFT studies.[17] The triple- ξ basis set 6–311 + G(d, p) and the hybrid functional B3LYP (Becke three-parameter Lee-Yang-Parr)[18] are used to optimize the initial geometry of the selected molecules.[19] The selected B3LYP functional is a hybrid functional with DFT exchange correlation parameters and 20% Hartree-Fock exchange, which makes it suitable for the selected cyclic amines.[18] The reason for selecting triple ξ premise set 6–311 + G(d, p) is its accuracy in calculations than the double-based basis set for the compounds having smaller sizes.[19] The vibrational frequency calculations are performed to check the minima of the S_0 optimized geometries of the cyclic amines. From the frequency calculations, the absence of imaginary frequency ensures the formation of lower energy coordinates. Further, the solvent effect of water has been considered by using integral equation formalism polarizable continuum model (IEFPCM) of Gaussian 09 software. Natural Bond Orbital (NBO) calculations are performed on the same level of theory, B3LYP/6-311 + G(d, p), to evaluate the natural population analysis. NBO predicts the charge, which plays a main role in determining the contribution of the amine group in the obtained $-\ln K_a$ values. The potential energy surface (PES) scanning plot is generated in $AEPZH^+$ molecule along the bond **N22-H25** with the step size of 0.2 Å in the ground state using B3LYP/6-311 + G(d, p) level of theory.

Results and Discussion

Experimental Results and Discussions

The first $-\ln K_a$ values of PZ experimentally determined between 298 and 318 K are summarized in Table 3 and compared with reported data of Hamborg et al.[13a] and Hetzer et al.[20] and it is deviate by 1.34% and 1.54% respectively. The experimentally determined $-\ln K_a$ values are in excellent agreement with the reported values.

Table 4 compares experimentally obtained and reported 2nd $-\ln K_a$ values of PZ within the range of 298–318 K. However, second $-\ln K_a$ values of PZ have a higher deviation from the data reported by Hamborg et al.[13a] (4.27%) and Hetzer et al.[20] (2.85%). Similar phenomenon is observed by Hartono et al.[21] and they reported that the value of second $-\ln K_a$ has more

Table 3. Experimentally obtained and already reported first $-\ln K_a$ values of PZ within the temperature range 298–318 K.

T, K	Present Work		Hamborg et al.[13a]	Hetzer et al.[20]
	pK_a	$-\ln K_a$		
298	9.56	22.02	22.37	22.41
303	9.44	21.80	22.08	22.13
308	9.39	21.62	21.8	21.81
313	9.28	21.44	21.53	21.57
318	9.03	21.00	21.27	21.3
△G KJ.mol^{-1}		54.58		
△H KJ.mol^{-1}		44.39		

Table 4. Experimentally obtained and already reported second $-\ln K_a$ values of PZ within the temperature range 298—318 K.

T, K	Present Work		Hamborg et al.[13a]	Hetzer et al.[20]
	pK_a	$-\ln K_a$		
298	5.18	11.93	12.45	12.28
303	5.08	11.78	12.24	12.08
308	5.01	11.49	12.03	11.87
313	4.93	11.38	11.83	11.66
318	4.85	11.23	11.63	11.47
△G KJ.mol^{-1}		29.57		
△H KJ.mol^{-1}		29.16		

Table 5. Experimentally obtained and already reported first $-\ln K_a$ values of 1-MPZ within the temperature range 298—318 K.

T, K	Present Work		Khalili et al.[15c]
	pK_a	$-\ln K_a$	
298	9.07	20.89	21.04
303	8.92	20.56	20.7
308	8.87	20.43	20.43
313	8.79	20.28	20.23
318	8.65	19.90	19.92
△G KJ.mol^{-1}		51.78	
△H KJ.mol^{-1}		35.13	

Table 6. Experimentally obtained and already reported second $-\ln K_a$ values of 1-MPZ within the temperature range 298–318 K.

T, K	Present Work		Khalili et al.[15c]
	pK_a	$-\ln K_a$	
298	4.48	10.32	10.66
303	4.42	10.22	10.31
308	4.38	10.08	10.09
313	4.33	10.01	9.92
318	4.27	9.82	9.83
△G KJ.mol^{-1}		25.58	
△H KJ.mol^{-1}		18.58	

deviation since it's measurement accounts the contribution of both monoprotonated and deprotonated amine molecules.

The experimentally evaluated value of first $-\ln K_a$ for 1-MPZ is summarized in Table 5. The estimated value of first $-\ln K_a$ for 1-MPZ is in good agreement with the reported data by Khalili et al.[15c] and deviation is 0.24%.

Table 6 summarizes the values of second $-\ln K_a$ of 1-MPZ within the studied temperature range and these are matching well with the existing reports by Khalili et al.[15c] and it is deviate only 0.68%.

PZ and 1-MPZ contain two amine (–NH) groups, and thus when titrated with HCl, two sharp changes in pH are shown in the titration plots represented in Figure 1(a) and (b). These plots represent typically for titration of PZ and 1-MPZ using 0.1 M HCl at 298 K–318 K.

Table 7 summarizes the obtained experimental values of $-\ln K_a$ for AEPZ in the temperature range of 298–318 K. The $-\ln K_a$ values for AEPZ is hardly available in literature and thus reported as new input in the present report. The trend of decreasing the $-\ln K_a$ with rise in temperature is observed also for AEPZ.

Table 7 includes the values of △G and △H estimated for dissociation of AEPZ using Equations (6) and (7). AEPZ contains three amine (–NH) groups. It seems reasonable to expect three $-\ln K_a$ values as well as three sharp changes in the pH of AEPZ when it is titrated with HCl. However, the titration of AEPZ with HCl at all the studied temperatures result single prominent steep change confirming the single $-\ln K_a$ value of AEPZ. In Figure 1(c), titration plots for AEPZ measured at 298, 303, 308, 313 and 318 K are shown. The underlying reasons for obtaining single $-\ln K_a$ value for AEPZ cannot be explained with the general rule of basicity and the same has been justified well with the restricted inversion model alongwith DFT calculation in the upcoming section. The reproducibility of experimentally obtained data for the $-\ln K_a$ of the investigated amines is provided in supporting information (Tables S3 and S4, Supporting Information for PZ, Tables S5 and S6, Supporting Information for 1 MPZ and Table S7, Supporting Information for AEPZ) for the reference.

The greater basic strength of the amines indicates it's higher rate of reactivity with acidic flue gas like CO_2. Comparing the

Table 7. Experimentally obtained and already reported $-\ln K_a$ values of AEPZ within the temperature range 298–318 K.

T, K	Present work	
	pK_a	$-\ln K_a$
298	9.58	22.07
303	8.82	20.32
308	8.63	19.96
313	8.57	19.74
318	8.35	19.23
△G KJ.mol^{-1}		54.70
△H KJ.mol^{-1}	(With 303–308 K)	55.83

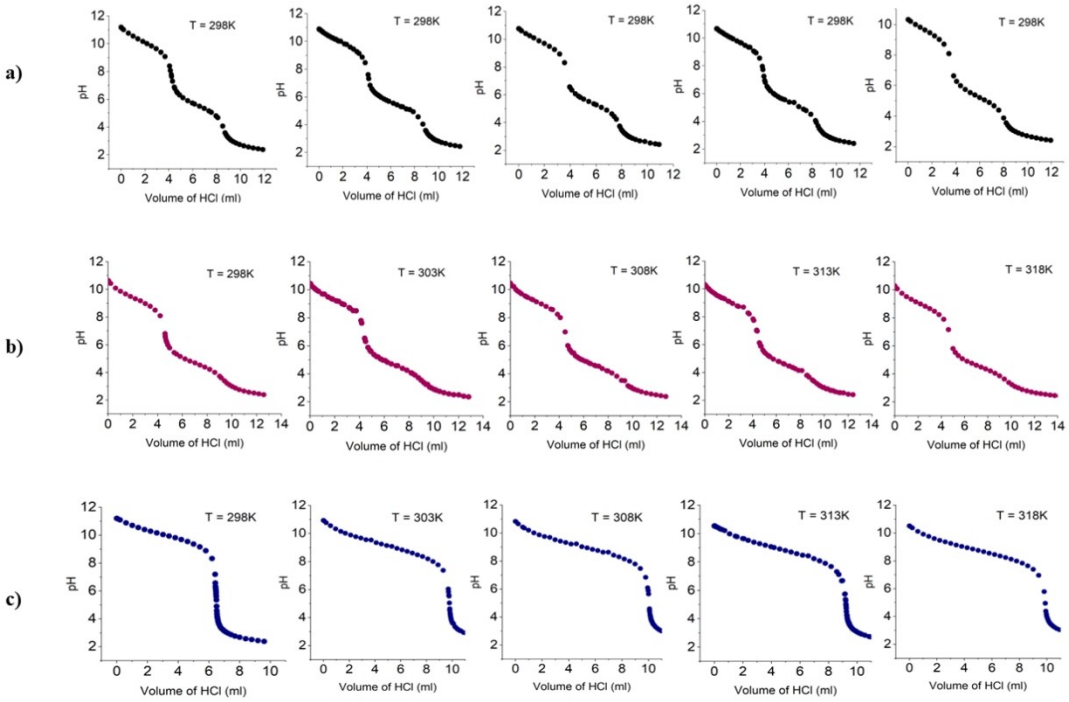

Figure 1. Plots for the titration of (a) PZ, (b) 1-MPZ, and (c) AEPZ using 0.1 M HCl at 298 to 318 K temperature.

$-\ln K_a$ values of AEPZ, it seems that AEPZ can also be a promising solvent for CO_2 absorption like PZ and 1-MPZ.

Computational Results and Discussions

Optimization

The S_0 optimized geometries of PZ, 1-MPZ, AEPZ, PZH^+, $PZ2H^+$, $1\text{-}MPZH^+$, $1\text{-}MPZ2H^+$, and $AEPZH^+$ are shown in Figure 2 (Tables S11–S18, Supporting Information). In the frequency calculations, these optimised geometries shows the absence of imaginary frequencies which confirms the formation of lower energy coordinates. Tables S8–S10, Supporting Information represents the optimised geometrical parameters of PZ, 1-MPZ, and AEPZ molecules. It can be observed from Tables S8–S10, Supporting Information that the obtained optimized geometrical parameters for PZ are in agreement with the reported literature.[22] On comparing the molecular structure of PZ with other two, 1-MPZ and AEPZ, it can be observed that they possess common piperazine scaffold. Based on this similarity, we compared the optimized geometrical parameters of 1-MPZ and AEPZ with PZ. It is clearly visible from the outcome (Tables S9 and S10, Supporting Information) that the three molecules possess similar geometrical parameters, thus it confirm the accuracy of the calculations, and these geometries were used for performing further calculations. The protonated forms (PZH^+, $PZ2H^+$, $1\text{-}MPZH^+$, $1\text{-}MPZ2H^+$, and $AEPZH^+$) of the selected amines also display the optimized geometrical parameters resembling with their counterparts.

NBO Analysis

In order to examine the distribution of charges on PZ, 1-MPZ, and AEPZ and their protonated counterparts, NBO calculations are carried out using B3LYP/6-311 + G(d, p) level of theory with IEFPCM solvation model. Figure 3 and Table 8 provide information on the natural charges generated on each atom of the molecules i.e. PZ, 1-MPZ, AEPZ, and their respective reduced forms PZH^+, $PZ2H^+$, $1\text{-}MPZH^+$, $1\text{-}MPZ2H^+$, and $AEPZH^+$. Among the three amines, the chemical structures of PZ and 1-MPZ molecules possess two Nitrogen (N) atoms in their scaffolds. From NBO calculations, it was observed that in case of optimized PZ, the two Nitrogen atoms (**N7** and **N8**) possess similar charge of −0.709. The similarity of the charges provides an equal probability of proton (**H17**) addition. Owing to the charge similarity, at first, we bind the H17 to **N7** atom (Figure 2) and the molecule is denoted as PZH^+. In the reduced form PZH^+, the charge on **N7** decreases to −0.541, whereas the

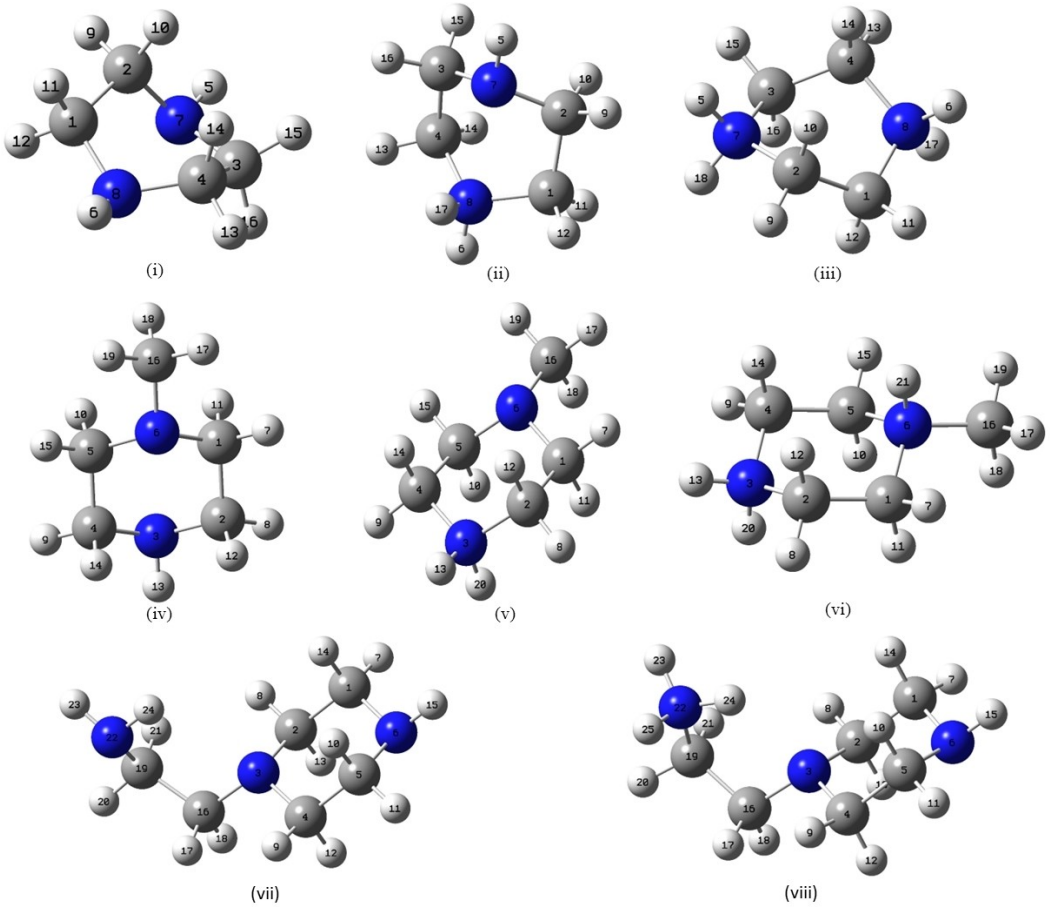

Figure 2. Optimized geometry of amine molecule. i) PZ, ii) PZH^+, iii) $PZ2H^+$, iv) 1-MPZ, v) 1-$MPZH^+$, vi) 1-$MPZ2H^+$, vii) AEPZ and viii) $AEPZH^+$ calculated at B3LYP/6-311 + G(d, p) with water solvent in IEFPCM solvation model.

charge on **N8** atom remains the same (−0.709) as shown in Table 8. Based on the electronegativity, the second proton (**H18**) is then attached to more electronegative **N8** in PZH^+ and the geometry is named as $PZ2H^+$. It is observed that on the addition of second proton ($PZ2H^+$), both **N7** and **N8** atoms attain the similar charge i.e. −0.545. Thus, based on charge analysis, the two $-\ln K_a$ values for PZ are verified with the experimental observations.

Similar to the structure of PZ, the molecular structure of 1-MPZ also comprises of two nitrogen atoms, i.e. **N3** and **N6** (Figure 2). However, in case of 1-MPZ, a methyl group is attached on one of the nitrogen atom (**N6**). Owing to the attachment of the **N6** atom to the methyl group, there is an uneven distribution of charge in the molecule (Figure 3), i.e., **N3** atom possesses a charge of −0.729 and **N6** display charge of −0.636. The higher charge on the **N3** atom favours the addition of the proton (**H_2O**), and the molecule is named as 1-$MPZH^+$. It is observed that the charge on both **N3** and **N6** atom decreases to −0.550, and 0.623 respectively. From the charge distribution analysis, among the two, **N6** is more electronegative in nature. Thus, the second proton is attached to the **N6** atom, and the geometry is named as 1-$MPZ2H^+$. The NBO charge distribution on the molecule 1-$MPZ2H^+$ displayed that the charge on **N3** and **N6** changes to −0.551 and −0.465, respectively. Thus in 1-$MPZ2H^+$, the proton will favourably attack on N3, followed by N6 atom, thus, validating the two −lnKa values obtained via experimental studies.

The AEPZ molecule has three nitrogen (**N3, N6**, and **N22**) atom in its structure (Figure 2), i.e., primary (**N22**), secondary (**N6**), and tertiary (**N3**). Unlike, 1-MPZ, this molecule has ethyl-amine substitution on one of the nitrogen (**N3**). Thus, all three nitrogen atoms shows uneven charge distribution in the molecule (Figure 3). The **N3** atom display charge of −0.602, **N6** atom display charge of −0.702, and **N22** atom display charge of −0.878. Thus, from the charge analysis, **N22** atom is more electronegative, thus, it is more prone to addition of proton (**H25**). The geometry obtained after adding a proton is denoted as $AEPZH^+$. It is observed that the charge decreased from −0.878 to −0.685 on **N22**, −0.702 to −0.700 on **N6**, whereas, it increases from −0.602 to −0.613 on **N3** (Figure 3). The different charge distribution on **N3**, **N6** and **N22** for monoprotonated AEPZ would enable further protonation which is experimentally not observed, and single protonation is already demonstrated in the titration plot. On analysing the geometry of mono-protonated AEPZ ($AEPZH^+$) molecule, it is observed that the molecule has attained the chair conformation shown in Figure 4. From the literature studies, it is confirmed that piperazine is stable in chair conformation,[23] and the chair conformation

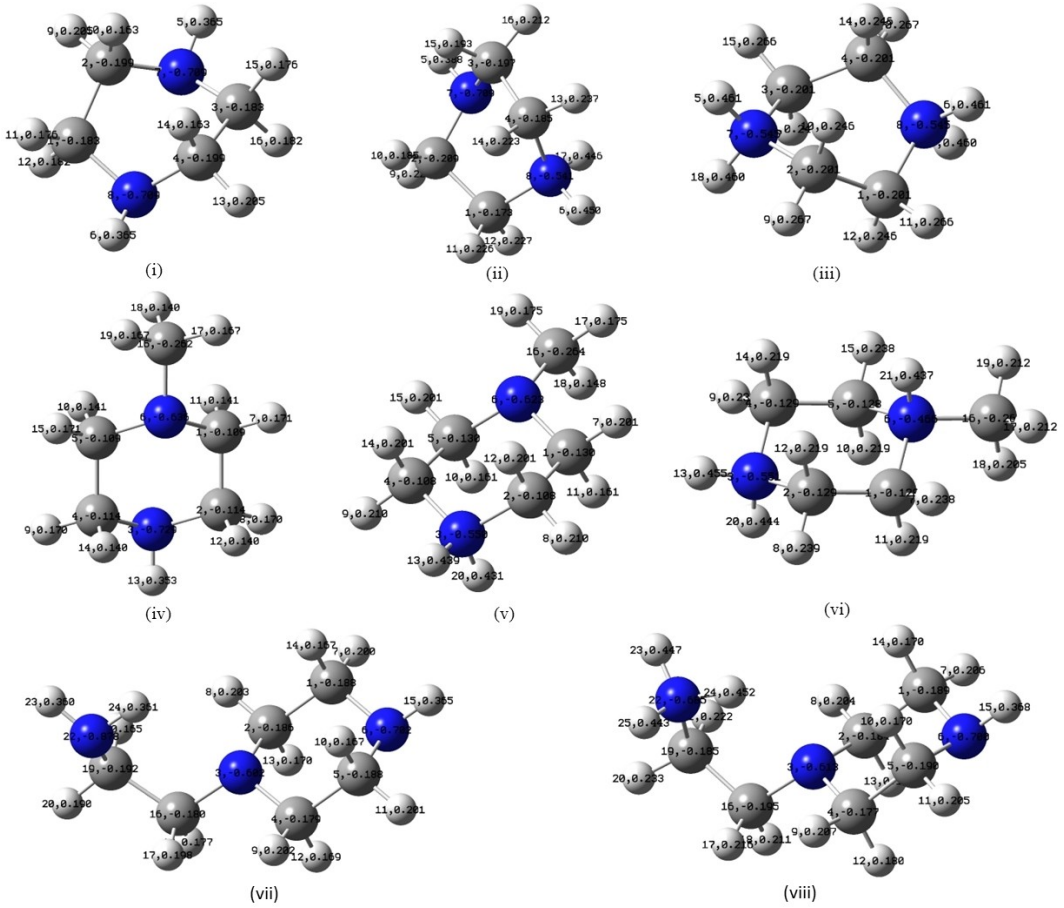

Figure 3. NBO charge distribution on amine molecule. i) PZ, ii) PZH^+, iii) $PZ2H^+$, iv) 1-MPZ, v) 1-$MPZH^+$, vi) 1-$MPZ2H^+$, vii) AEPZ and viii) $AEPZH^+$ calculated B3LYP/6-311 + G(d, p) with water solvent in IEFPCM solvation model.

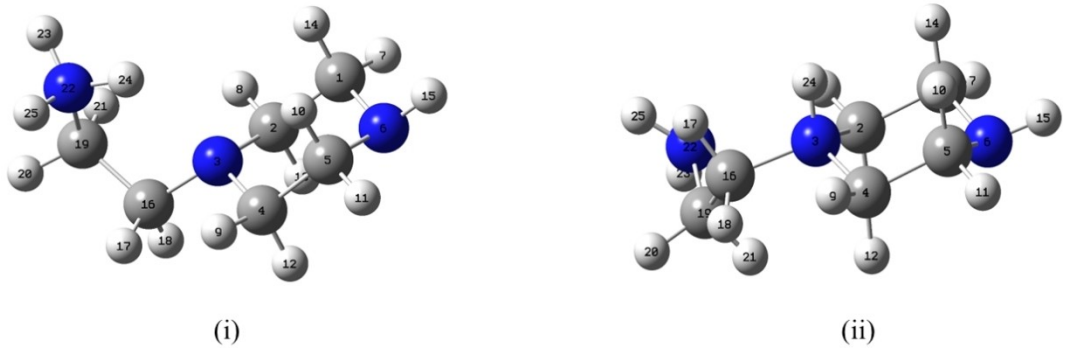

Figure 4. Ring inversion of $AEPZH^+$ retrieved from PES calculations conducted at B3LYP/6-311 + G(d, p) with water solvent in IEFPCM solvation model.

facilitate the ring inversion process.[24] In order to confirm the same, the potential energy scanning plots were generated and energy was calculated for both the normal and inverted conformations of $AEPZH^+$ (Figure 5). It was observed that both normal and inverted conformations of $AEPZH^+$ possess energy of −402.4172 Hartree (2.5×10^{-5} kcal/mol). This supports the rapid interconversion of one chair conformation to another (ring inversion). The rapid interconversion between the two chair forms at room temperature has also been reported in the literature.[24] The single pK_a value of AEPZ thus can be justified based on the conformation inversion model along with DFT calculation and literature report. Further, DFT calculations of potential energy surface (PES) scans are performed on $AEPZH^+$ as the function of **N22**-**H24** bond length with the step size of 0.2 Å in the ground state (Figure 5). Interestingly, it is observed that as soon as **H25** form binding with **N22** ($AEPZH^+$), the bond length between the **N22** and **H24** increases (Figure 2, Table S10, Supporting Information). Therefore, in the PES plots, the **N22**-**H24** bond length was considered. From the PES plot displayed in the Figure 5, it is observed that the molecule attains ring

Table 8. Calculated NBO charge distribution of the selected amine molecule calculated at B3LYP/6-311 + G(d, p) with water solvent in IEFPCM solvation model.

Atom	PZ	PZH^+	$PZ2H^+$
C1	−0.183	−0.197	−0.201
C2	−0.199	−0.185	−0.201
N7	**−0.709**	**−0.541**	**−0.545**
C3	−0.183	−0.173	−0.201
C4	−0.199	−0.209	−0.201
N8	**−0.709**	**−0.709**	**−0.545**
	1-MPZ	**1-MPZH$^+$**	**1-MPZ2H$^+$**
C1	−0.109	−0.130	−0.128
C2	−0.114	−0.108	−0.129
N3	**−0.729**	**−0.550**	**−0.551**
C4	−0.114	−0.108	−0.129
C5	−0.109	−0.130	−0.128
N6	**−0.636**	**−0.623**	**−0.465**
C16	−0.262	−0.264	0.261
	AEPZ	**AEPZH$^+$**	
C1	−0.188	−0.189	
C2	−0.186	−0.184	
N3	**−0.602**	**−0.613**	
C4	−0.179	−0.177	
C5	−0.188	−0.190	
N6	**−0.702**	**−0.700**	
C16	−0.180	−0.195	
C19	−0.192	−0.185	
N22	**−0.878**	**−0.685**	

The bold data shows change in charge for nitrogen atom in PZ, 1-MPZ, and AEPZ

Table 9. Calculated bond length of nitrogen and proton (H^+) of the amine product calculated at B3LYP/6-311 + G(d, p) with water solvent in IEFPCM solvation model.

Amine	Bonding atom	Bond length (Å)
PZ	N7-H17	1.02
	N8-H18	1.02
1-MPZ	N3-H20	1.00
	N6-H21	1.00
AEPZ	N22-H25	1.02

inversion in step 13. In the scanning plot, geometry generated at step 5 displayed the stable geometry. It is observed that the bond length between the **N22** and **H24** increases with each step and at step 5, it forms stable bond with **N3** with bond length of 1.04 Å. Thus, on the addition of **H25**, the molecule $AEPZH^+$ showed intramolecular proton transfer (IMPT) (Figure 5). After the formation of IMPT, the conformation of the molecule changes and in step 13, it displayed ring inversion (Figure 5). Thus, we can predict that IMPT causes ring inversion in the molecule which is further responsible for single pK_a value of AEPZ. The calculated bond length of nitrogen and H^+ of PZ, 1-MPZ, AEPZ is given in Table 9.

Conclusions

Present work deals with the experimental investigation on dissociation constants of dibasic cyclic di-amine PZ, MPZ and tribasic amines AEPZ which is an essential property when these amines are used for CO_2 capture solvent. Experimental findings are justified based on DFT calculations. Potentiometric titration method is used to estimate the dissociation constant of studied amines. The obtained first and second dissociation constants of the PZ are 22.02, and 11.93 respectively at 298 K. Similarly, the first and second dissociation constant of 1-MPZ are 20.89, and 10.32 respectively at 298 K. The dissociation constants of AEPZ are 22.07, 20.66, 20.38, 20.2, and 19.86 at temperature range (298–318 K). The geometry of the investigated amine solvents are optimized using Density functional theory (DFT) calculations using B3LYP/6-311 + G(d, p) with water solvent in IEFPCM solvation model in the ground state. The optimised geometrical parameters and the charge distribution among the nitrogen and other elements are calculated. The charge calculation helps in identifying the atom involved in forming hydrogen bonds in the molecule. It is observed that, dibasic PZ and 1-MPZ both show two distinct pK_a values which can be explained easily based on the general rule of basicity and also validated through the charge analysis. In case of tribasic AEPZ, only one pK_a value was obtained. From the NBO analysis, we confirm the formation of hydrogen bonding (**H25**) with the primary amine in the molecule, however, due to IMPT, the inherent proton (**H24**) of the primary amine form hydrogen bonding with the tertiary amine of the molecule, which further lead to ring inversion of the piperazine moiety. The IMPT was explained with the help of PES plots, and it validates the single pK_a value of tribasic AEPZ molecule.

Conflict of Interests

The authors declare that there is no potential for a conflict of interest.

Authorship Contribution

Mehul Darji: Formal analysis; Investigation; Methodology; Computational DFT study; Writing-original draft; Review & editing. **Anu Manhas**: Supervision on computational DFT study; **Sukanta K. Dash**: Conceptualization; Funding acquisition; Project administration; supervision, Resources, review & editing: **Kalisadhan Mukherjee**: Supervision; Conceptualization, Data analysis; Writing- review & editing.

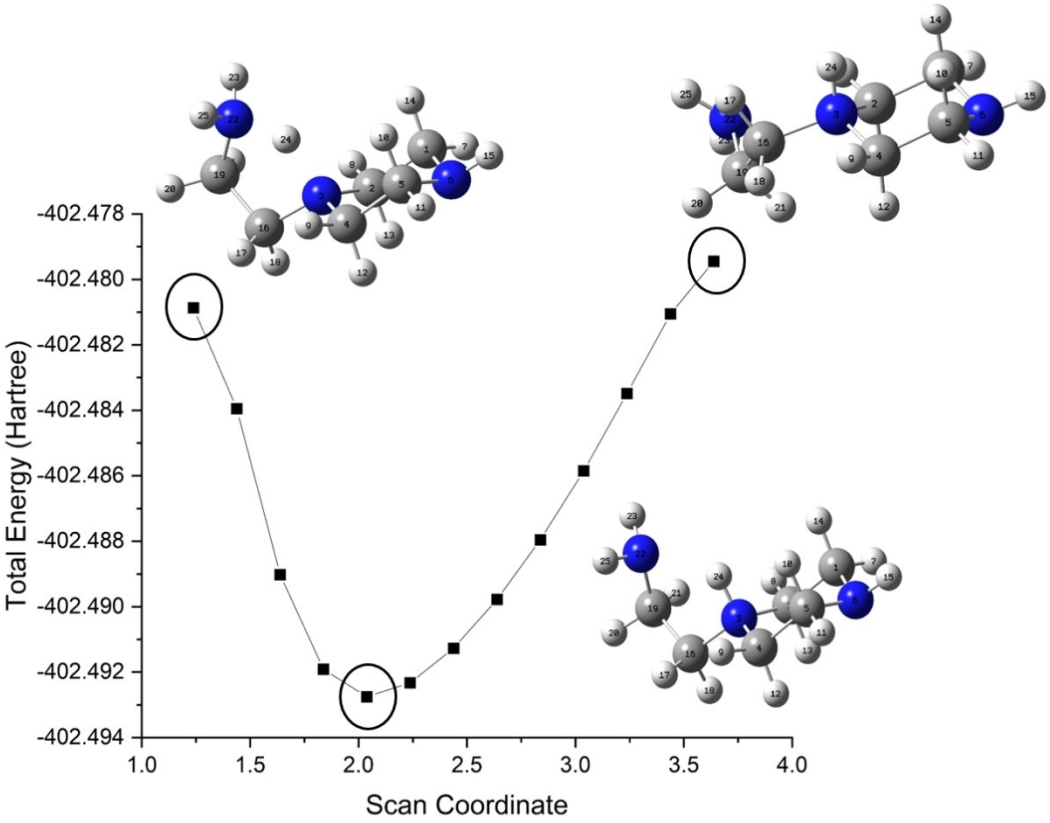

Figure 5. Potential energy scanning curves of the ground sate geometry of $AEPZH^+$ as the function of bond length N22-H24 calculated at B3LYP/6-311 + G(d, p) with water solvent in IEFPCM solvation model.

Abbreviations

MEA	Monoethanolamine
AMP	2-Amino-2-methyl-1-propenol
PZ	Piperazine
1-MPZ	1-Methyl piperazine
AEPZ	1-(2-aminoethyl)piperazine
VLE	Vapour liquid equilibrium

Acknowledgements

Mehul Darji sincerely acknowledges the fellowship support from SHODH scheme, Govt. of Gujarat, India.

Conflict of Interest

The authors declare no conflict of interest.

Data Availability Statement

The data that support the findings of this study are available in the supplementary material of this article.

Keywords: Amine solvent · CO_2 capture · Density functional calculations · Dissociation constant · and Potentiometric titration

[1] a) V. Masson-Delmotte, P. Zhai, H.-O. Pörtner, D. Roberts, J. Skea, P. R. Shukla, A. Pirani, W. Moufouma-Okia, C. Péan, R. Pidcock, *An IPCC Special Report on the impacts of global warming of 2018*, *1*, 43–50; b) M. Bui, C. S. Adjiman, A. Bardow, E. J. Anthony, A. Boston, S. Brown, P. S. Fennell, S. Fuss, A. Galindo, L. A. Hackett, *Energy Environ. Sci.* **2018**, *11*, 1062–1176.
[2] a) M. Bui, N. Mac Dowell, *Carbon Capture and storage*, Royal Society of Chemistry, London **2019**; b) V. Becattini, P. Gabrielli, M. Mazzotti, *Ind. Eng. Chem. Res.* **2021**, *60*, 6848–6862; c) C. Shukla, P. Mishra, S. K. Dash, *Front. Energy Res.* **2023**, *11*, 1135188; d) S. K. Dash, S. S. Bandyopadhyay, *Int. J. Greenhouse Gas Control* **2016**, *44*, 227–237; e) S. K. Dash, A. N. Samanta, S. S. Bandyopadhyay, *Int. J. Greenhouse Gas Control* **2014**, *21*, 130–139.
[3] a) N. H. Khdary, A. S. Alayyar, L. M. Alsarhan, S. Alshihri, M. Mokhtar, *Catalysts* **2022**, *12*, 300; b) M. M. M. Mostafa, W. Bajafar, L. Gu, K. Narasimharao, M. Abdel Salam, A. Alshehri, N. H. Khdary, S. Al-Faifi, A. D. Chowdhury, *Catalysts* **2022**, *12*, 893; c) M. M. M. Mostafa, A. Shawky, S. F. Zaman, K. Narasimharao, M. Abdel Salam, A. A. Alshehri, N. H. Khdary, S. Al-Faifi, A. D. Chowdhury, *Catalysts* **2022**, *12*, 1479; d) K. I. Assaf, A. K. Qaroush, F. M. Mustafa, F. Alsoubani, T. M. Pehl, C. Troll, B. Rieger, A. a. F. Eftaiha, *ACS Omega* **2019**, *4*, 11532–11539; e) W. Wang, M. Zhou, D. Yuan, *J. Mater. Chem. A* **2017**, *5*, 1334–1347.
[4] S. K. Dash, R. Parikh, D. Kaul, *Mater. Today:. Proc.* **2022**, *62*, 7072–7076.
[5] a) S. K. Dash, A. N. Samanta, S. S. Bandyopadhyay, *Fluid Phase Equilib.* **2011**, *307*, 166–174; b) S. K. Dash, A. N. Samanta, S. S. Bandyopadhyay, *J. Chem. Thermodyn.* **2012**, *51*, 120–125.
[6] Y. Liu, L. Zhang, S. Watanasiri, *Ind. Eng. Chem. Res.* **1999**, *38*, 2080–2090.
[7] M. Darji, A. Manhas, S. K. Dash, K. Mukherjee, *Ind. Eng. Chem. Res.* **2023**, *62*, 7868–7876.

[8] a) A. Dey, S. K. Dash, S. C. Balchandani, B. Mandal, *J. Mol. Liq.* **2019**, *289*, 111036; b) I. S. Sukanta Kumar Dash, *Environmental Science Pollution Resarch* **2023**, 1–15.
[9] S. K. Dash, A. Samanta, A. N. Samanta, S. S. Bandyopadhyay, *Fluid Phase Equilib.* **2011**, *300*, 145–154.
[10] J. T. Cullinane, G. T. Rochelle, *Ind. Eng. Chem. Res.* **2006**, *45*, 2531–2545.
[11] H. Li, Y. Le Moullec, J. Lu, J. Chen, J. C. V. Marcos, G. Chen, F. Chopin, *Fluid Phase Equilib.* **2015**, *394*, 118–128.
[12] A. V. Rayer, K. Z. Sumon, A. Henni, P. Tontiwachwuthikul, *Energy Procedia* **2011**, *4*, 140–147.
[13] a) E. S. Hamborg, G. F. Versteeg, *J. Chem. Eng. Data* **2009**, *54*, 1318–1328; b) E. S. Hamborg, J. P. Niederer, G. F. Versteeg, *J. Chem. Eng. Data* **2007**, *52*, 2491–2502.
[14] D. Wang, J. Xie, G. Li, W. Meng, J. Li, D. Li, H. Zhou, *ACS Omega* **2022**, *7*, 2897–2907.
[15] a) A. Tagiuri, M. Mohamedali, A. Henni, *J. Chem. Eng. Data* **2016**, *61*, 247–254; b) W. H. C. H. Nguyen, A. Henni, *J. Chem. Eng. Data* **2020**, *65*, 2280–2290; c) F. Khalili, A. Henni, A. L. East, *J. Chem. Eng. Data* **2009**, *54*, 2914–2917.
[16] a) S. Ma'mun, D. Kurniawan, E. Amelia, V. Rahmat, D. R. Alwani, in *MATEC Web of Conferences* **2017**, p. 02001; b) S. Ma'mun, J. P. Jakobsen, H. F. Svendsen, O. Juliussen, *Ind. Eng. Chem. Res.* **2006**, *45*, 2505–2512.
[17] A. Frisch, Wallingford, USA, 25p **2009**, *470*.
[18] I. Y. Zhang, J. Wu, X. Xu, *Chem. Commun.* **2010**, *46*, 3057–3070.
[19] M. P. Andersson, P. Uvdal, *J. Phys. Chem. A* **2005**, *109*, 2937–2941.
[20] H. B. Hetzer, R. Robinson, R. G. Bates, *J. Phys. Chem.* **1968**, *72*, 2081–2086.
[21] A. Hartono, E. F. da Silva, H. Grasdalen, H. F. Svendsen, *Ind. Eng. Chem. Res.* **2007**, *46*, 249–254.
[22] B. R. Srinivasan, A. R. Naik, M. Poisot, C. Näther, W. Bensch, *Polyhedron* **2009**, *28*, 1379–1385.
[23] S. SenGupta, N. Maiti, R. Chadha, S. Kapoor, *Chem. Phys.* **2014**, *436*, 55–62.
[24] S. S. Gupta, *Basic Stereochemistry of Organic Molecules*, Oxford University Press, United Kingdom **2018**.

Manuscript received: October 3, 2023